Journal of Applied Polymer Science

Electrospun Heat Management Polymeric Materials of Interest in Food Refrigeration and Packaging

Wilson Chalco-Sandoval, María José Fabra, Amparo López-Rubio, Jose M. Lagaron
Novel Materials and Nanotechnology Group, IATA-CSIC, 46980 Paterna (Valencia), Spain
Correspondence to: J. M. Lagaron (E-mail: lagaron@iata.csic.es)

ABSTRACT: The use of latent heat storage materials using phase change materials (PCMs) is an effective way of buffering thermal fluctuations and has the advantages of high-energy storage density and the isothermal nature of the storage process. The aim of this work was to develop slabs with energy storage capacity for their application in refrigerated foods. To this end, polycaprolactone (PCL) and polystyrene (PS) were used as encapsulating matrices of a PCM, specifically RT5 (a paraffin which has a transition temperature at 5°C), by using electrohydrodynamic processing. The effect of storage temperature (4°C and 25°C) and time on the morphology and thermal characteristics of the PCL/RT5 and PS/RT5 slabs was evaluated. Results showed that RT5 can be properly encapsulated inside both polymers, although PCL provided better encapsulation efficiency. Encapsulation efficiency was affected not only by the polymer matrix but also by storage time at 25°C. The greatest encapsulation efficiency (98.6%) and optimum heat management performance was achieved for PCL/PCM slabs stored at 4°C, corresponding to materials composed of ~44 wt % of PCM (core material) and ~56 wt % of the PCL shell material. These temperature buffering materials can be of great interest to preserve the quality of packaged foods and to increase efficiency and reduce energy consumption in refrigeration equipment. © 2014 Wiley Periodicals, Inc. J. Appl. Polym. Sci. **2014**, *131*, 40661.

KEYWORDS: biopolymers and renewable polymers; crystallization; differential scanning calorimetry (DSC); fibers; polystyrene

Received 23 January 2014; accepted 27 February 2014
DOI: 10.1002/app.40661

INTRODUCTION

Refrigeration systems have been used during the last decades as a main method of food preservation. In fact, it is well-known that frozen and freezing temperatures are required during transport and storage in order to maintain the quality and safety of many foodstuffs. It is worth to note that food quality is often compromised by temperature fluctuations during food commercialization which, amongst others, contributes to the formation of heterogeneous crystal growth.

However, refrigeration is one of the heavy energy consumers. Furthermore, the ozone layer depletion and greenhouse gases emission associated to the use of air conditioners and refrigerators that make use of chlorofluorocarbons and hydrochlorofluorocarbons (CFCs and HCFCs) as refrigerants represent great environmental concerns. The phase-out of CFCs and HCFCs according to the Montreal Protocol urges the researchers to find out environmentally friendly new substitutes for refrigerants or novel technologies to reduce the amount of refrigerant used in these systems as well as to reduce the energy consuption of these.

As a result, researchers are focused on developing technical options for improving the energy performance of household refrigerators and one of the most innovative options is the use of phase change materials (PCMs).

PCMs are substances that undergo a phase transition at a specific temperature and, as a result, they are able to absorb and release the latent heat when isothermal conditions are altered.[1] PCMs could be used during transport or storage, for the protection of solid foods, beverages, pharmaceutical products, textile industry, blood derivatives, electronic circuits, cooked food, biomedical products, and many others.[2] The most commonly used PCMs are paraffin waxes, fatty acids, eutectics, and hydrated salts.[3] The paraffin compounds fulfil most of the requirements for being used as PCMs, as they are reliable, predictable, nontoxic, chemically inert, and stable below 500°C. They also show little volume changes on melting and have low vapour pressure in the molten form.[4] On the other hand, the inorganic substances, like salt hydrates, usually suffer from supercooling and phase separation during their applications which often compromises the temperature buffering behavior of these materials and cause random variations or progressive drifting of the transition zone over repeated phase change cycles. Furthermore, corrosion is another shortcoming of these materials.[5]

Direct application of PCMs is difficult because they have weak thermal stability, low thermal conductivity, and some of them are liquid at ambient temperature and, thus, are not easy to handle or to be directly incorporated into packaging structures and refrigeration equipments.[6] Therefore, the encapsulation of the PCM in a shell material is a plausible solution to avoid all these problems. Microencapsulated PCM is a form of PCM encapsulated in natural and synthetic polymeric capsules, which range in size from less than 1 μm to more than 1000 μm. The microcapsules protect the PCM against the influences of the outside environment, increasing the heat-transfer area, and permitting the core material to withstand changes in volume of the PCM, as the phase change occurs allowing small and portable thermal energy storage systems.[5]

One methodology being increasingly used for the microencapsulation of materials is electrohydrodynamic processing. This processing technique has proven to be a suitable method for encapsulation of several components, including biomedical substances, functional food ingredients, PCMs, and others substances within polymer matrices.[7–9] The electrohydrodynamic processing commonly termed as electrospinning is a technique whereby long nonwoven ultrafine structures, typically fibers with diameters of several tens to several hundreds of nanometers, may be formed by applying a high-voltage electric field to a solution containing polymers.[10] The basic principle of electrospinning is to apply high voltage on the polymer solution or melt that would overcome polymer surface tension and induce the jet formation. Applied tip-to-collector electric field causes surface charge repulsion of solution which deforms spherical drop of viscoelastic polymer solution on needle tip into conical shape (Taylor's cone). When electrostatic forces of surface charge repulsion overcome polymer surface tension, charged jet ejects from Taylor's cone and deforms uniaxially through electric field toward grounded collector. Simultaneously, with rapid whipping of the jet, the evaporation of the solvent leaves dried fibers behind.[11] It is believed that higher electric field causes spreading of main jet into numerous secondary fibers with smaller approximately equal diameter regarding the main jet. Due to instability of polymer jet, deformation depends on the electric field strength. Therefore, it is necessary to adjust electrospinning parameters for uniform nanofibers fabrication. To produce fibers, a large number of highly specific conditions including solution properties (polymer concentration, viscosity, electrical conductivity, surface tension, and solvent volatility), environmental conditions (temperature, air velocity, and humidity), and process conditions (voltage, spinning distance, and flow rate) must be met.

The aim of this work was, on one hand, to develop heat management materials based on the encapsulation of a PCM which melts at 5°C (RT5—core material) inside two different polymeric matrices (polycaprolactone (PCL) and polystyrene (PS)) (shell material) by means of the electrohydrodynamic processing and, on the other hand, to study the effects of storage temperature and ageing on the performance of these PS/RT5 and PCL/RT5 slabs. It is important to understand how these materials will behave as a function of temperature and time, because these encapsulated structures are aimed to be introduced in packaging structures or in refrigeration equipments, in order to counteract temperature fluctuations and to increase the energetic efficiency of the devices, respectively.

MATERIALS AND METHODS

Materials

Rubitherm RT5, a technical grade paraffin wax, was chosen as the PCM for cool storage. It is based on a cut resulting from refinery production and it consists entirely of normal paraffin waxes (C14-C18). RT5 was purchased from Rubitherm Technologies GmbH (Berlin, Germany). The PCL grade FB100 was supplied by Solvay Chemicals (Belgium). PS commercial grade foam was supplied by NBM (Valencia, Spain). *N*,*N*-dimethylformamide (DMF) with 99% purity and trichloromethane (99%) were purchased from Panreac Quimica S.A. (Castellar del Vallés, Spain). All products were used as received without further purification.

Preparation of Films

Preparation of PS/PCM and PCL/PCM Solutions. The electrospinning solutions were prepared by dissolving the required amount of PS and PCL, under magnetic stirring, in a solvent prepared with a mixture of trichloromethane : DMF (70 : 30 w/w) in order to reach a 10% or 13% in weight (wt %) of PS or PCL, respectively. Afterward, 45 wt % of PCM (Rubitherm 5) with respect to the polymer weight was added to the polymer solutions, and stirred at room temperature until it was completely dissolved.

Electrohydrodynamic Processing. The full process of the PCM encapsulation through electrohydrodynamic processing has been previously developed (patent application number: P201131063). Based on previous knowledge, PCL/PCM and PS/PCM solutions were prepared according to Pérez-Masiá et al.,[9] in order to produce fibrillar structures. Thus, PCMs were microencapsulated within two different polymeric matrices (PS and PCL) by means of a Fluidnatek® electrospinning pilot plant tool from Bioinicia S.L. (Valencia, Spain) equipped with a variable high-voltage 0–60 kV power supply. PCL/PCM or PS/PCM solutions were electrospun under a steady flow-rate using a motorized high throughput multinozzle injector, scanning horizontally toward a metallic grid used as collector. The electrospinning conditions for obtaining both PCM-containing polymer structures were optimized and fixed at 55 mL/h of flow-rate, tip-collector distance of 26 cm, and the voltage of the collector and injector were set at 52 kV and 44 kV, respectively.

Preparation of PS/RT5 and PCL/RT5 Slabs. Based on screening studies (data not shown) on the energy storage capacity of electrospun fiber mats, PS/RT5 and PCL/RT5 slabs (3 × 1 × 1 cm) were developed in order to increase the temperature buffering capacity of the materials. To this end, the electrospun fiber mats, obtained in a pilot plant electrospinning equipment, were slightly pressed using a hot-plate hydraulic press at 63°C for 90 s.

Slabs Conditioning and Storage. Samples were equilibrated in desiccators at 0% HR by using silica gel and at two different temperatures 4°C and 25°C for 3 months. PCL/PCM and PS/PCM slabs were taken from the desiccators stored at 4°C and 25°C at different time intervals (0, 7, 15, 30, 45, 60, and 90

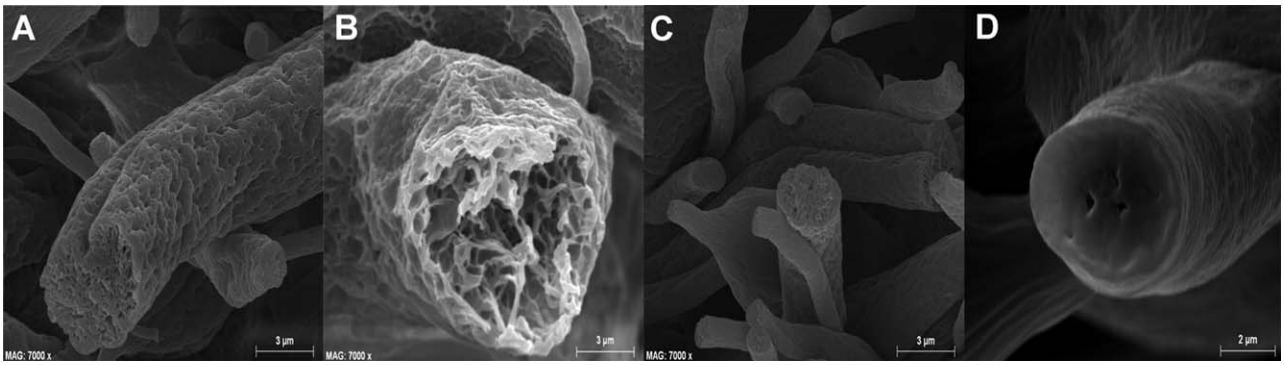

Figure 1. SEM images of electrospun fibers: (A) polystyrene/PCM, (B) polycaprolactone/PCM, (C) control polystyrene fibers, and (D) control polycaprolactone fibers.

days) and differential scanning calorimetry (DSC) and Fourier transform infrared (FTIR) analysis were carried out.

Characterization of Slabs

Scanning Electron Microscopy (SEM). The morphology of the electrospun PCL/PCM and PS/PCL fibers and slabs was examined using SEM on a Hitachi microscope (Hitachi S-4100). Samples were frozen in liquid N_2 and cryofractured to observe the cross section of the samples. Then, they were fixed to beveled holders using conductive double side adhesive tape, sputtered with a mixture of gold-palladium, and observed using an accelerating voltage of 10 kV. The diameters of the electrospun mats were measured by means of the Adobe Photoshop CS4 software from the SEM micrographs in their original magnification. The calculation of the number-average diameter was done by measuring 300 fibers diameters.

Differential Scanning Calorimetry. Thermal analyses of electrospun fibers and slabs were carried out on a DSC analyzer (Perkin Elmer DSC 7, US) from −20 to 20°C in a nitrogen atmosphere using a refrigerating cooling accessory (Intracooler 2, Perkin Elmer, US). The scanning rate was 2°C/min in order to minimize the influence of this parameter in the thermal properties. The amount of material used for the DSC experiments was adjusted so as to have a theoretical PCM content of 1–2 mg approximately. The enthalpy results obtained were, thus, corrected according to this PCM content. All tests were carried out, at least, in duplicate.

Attenuated Total Reflectance Infrared Spectroscopy. Attenuated total reflectance infrared spectroscopy (ATR-FTIR) spectra of polymers (PCL and PS), pure RT5 and PCL/PCM and PS/PCM slabs were collected at 25°C in a FTIR Tensor 37 equipment (Bruker, Germany). The spectra were collected in the different materials by averaging 20 scans at 4 cm^{-1} resolution. The experiments were repeated twice to verify that the spectra were consistent between individual.

Temperature Profiles. The temperature profiles of slabs with and without PCM were compared. To this end, PCL and PS slabs were frozen at −18°C for 1 day. Then, the surface temperature was registered at room temperature (20°C) by using an infrared thermometer MS Plus provided by PCE Instruments (Tobarra, Spain).

Statistical Analysis

A statistical analysis of data was performed through analysis of variance (ANOVA) using Statgraphics Plus for Windows 5.1 (Manugistics Corp., Rockville, MD). Homogeneous sample groups were obtained by using LSD test (95% significant level).

RESULTS

Morphology

The morphology of the electrospun structures was analyzed through SEM. Microstructural images provide information about the morphology of the slabs and allow us to gain a better understanding of thermal properties of slabs. Initially, the morphology of PS/PCM (a) and PCL/PCM (b) fibers were observed because the microstructure of the fibers could aid to explain the encapsulation efficiency of the different materials, as well as their thermal performance during storage time. Figure 1 shows the cross sections of both cryofractured fibers. Control PCL and PS fibers are also included for comparison purposes.

From these images, it can be observed that the incorporation of RT5 led to the formation of several channels inside the fibrillar structures where the PCM was supposed to be allocated (compare with PS and PCL control fibers in Figure 1(C,D), respectively, where no such channels were observed). These channels were much bigger in PCL/PCM structures than in PS/PCM electrospun fibers, which could help explain the differences in thermal properties as it will be detailed below. Noticeable differences were observed between both types of fibers. PCL/PCM fibers were thicker and both encapsulation structures presented a porous surface, although in the case of PS/PCM fibers, pore size was much smaller. There are several studies which indicate that the use of volatile solvents or high relative humidity can contribute to produce porous nanofibers.[12–16] However, in this study, the porous structure is thought to derive from the encapsulation of the PCM because the fibers with no PCM did not exhibited such a porous structure. In fact, the pores were actually the areas where the PCM was most likely to be located and, therefore, account for the capsule size obtained by the processing technique.

Figures 2 and 3 show the surface (a–c) and cross sections (a′–c′) of nonstored and stored (at 4 and 25°C) slabs of

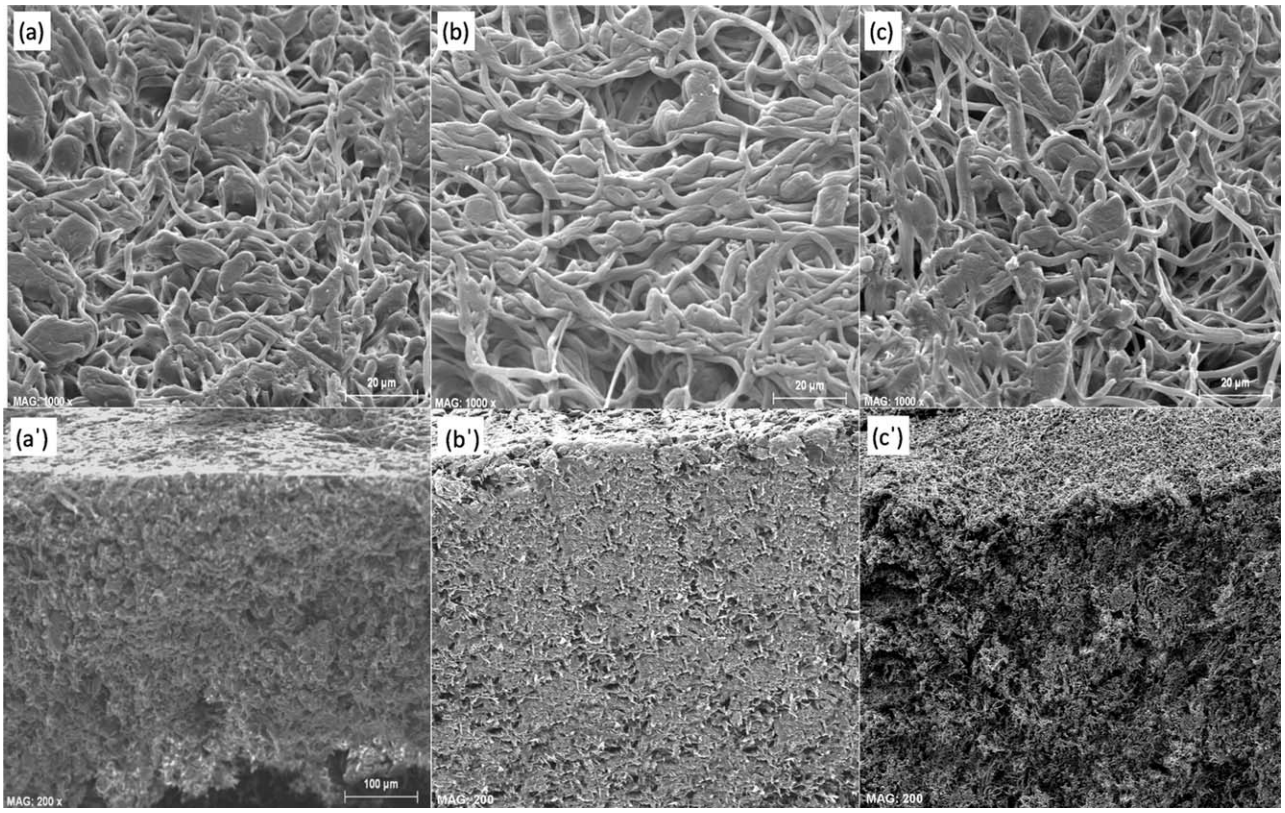

Figure 2. SEM images of surface (a–c) and cross-section (a′–c′) of electrospun PS/PCM fibers: (a–a′) nonstored slabs, (b–b′) stored slabs for 3 months at 4°C, (c–c′) stored slabs for 3 months at 25°C.

PS/PCM and PCL/PCM, respectively. From surface images, it is clearly observed that the fibers obtained from the PCL/PCM solution were thicker (fiber diameters ranged from 0.55 to 11.91 μm), whereas in PS/PCM slabs, many beaded areas (1.96–19.77 μm) were distinguished within the fibrous mats and not significant morphological differences were observed between nonstored and stored slabs (diameter of fibers ranged from 0.35 to 3.89 μm).

Remarkable changes can be discerned from the cross-section images. Nonstored PS/PCM [Figure 2(a′)] and PCL/PCM [Figure 3(a′)] slabs were more compact than the ones stored at 25°C [Figures 2(c′) and 3(c′)]. However, the appearance of slabs stored at 4°C [Figures 2(b′) and 3(b′)] was similar to that observed for nonstored slabs, probably due to the physical state of the PCM. As commented on above, the phase transitions of RT5 take place around 5°C and, thus, the PCM was in a solid state at 4°C and remained in the porous structure during storage. On the opposite, PCM was in a liquid state at room temperature (25°C), which clearly contributed to modify the structure of the slabs. In this sense, it is worth to note that stored PCL/PCM slabs at 25°C were delaminated after 3 months, probably due to the morphology of fibers which facilitated the PCM (which was liquid at room temperature) migration out of the encapsulating pores.

Thermal Properties of Electrospun Structures

The thermal behavior of the PCL/PCM and PS/PCM structures was analyzed by DSC and it was also used to ascertain the degree of PCM incorporation. First, the thermal behavior of pure RT5 is shown in Figure 4.

The PCM melted at ~7.20°C and crystallized at ~5.26°C, in a narrow temperature range, having an enthalpy of 144.7 J/g. However, the thermal properties of RT5 varied when this PCM was encapsulated within the polymer (PS or PCL) matrices and upon ageing.

Thermal properties (enthalpy values, melting and crystallization temperatures, and supercooling degree) of the internal and external parts of the PS/RT5 slabs analyzed by DSC at 2°C min^{-1} are given in Tables I and II, respectively. Similarly, the corresponding data of internal and external parts of PCL/PCM slabs are displayed in Tables III and IV, respectively.

From Tables I and II, it can be observed that when RT5 was encapsulated in the PS matrix, the melting enthalpy was lower than that of the nonencapsulated PCM. This difference could be explained by part of the PCM not being properly encapsulated, and/or by an interaction of the PCM with the encapsulating polymer, thus partially hindering paraffin crystallization. As expected, the crystallization and melting enthalpy of slabs were significantly higher at the internal part of the slabs, probably due to the slight heat-treatment suffered from the outer zones during the slab-formation. On the other hand, the melting temperature of pure RT5 was in the same range as the melting temperature of the slabs, indicating that similar PCM crystals were formed in the encapsulation structures. Furthermore, in the

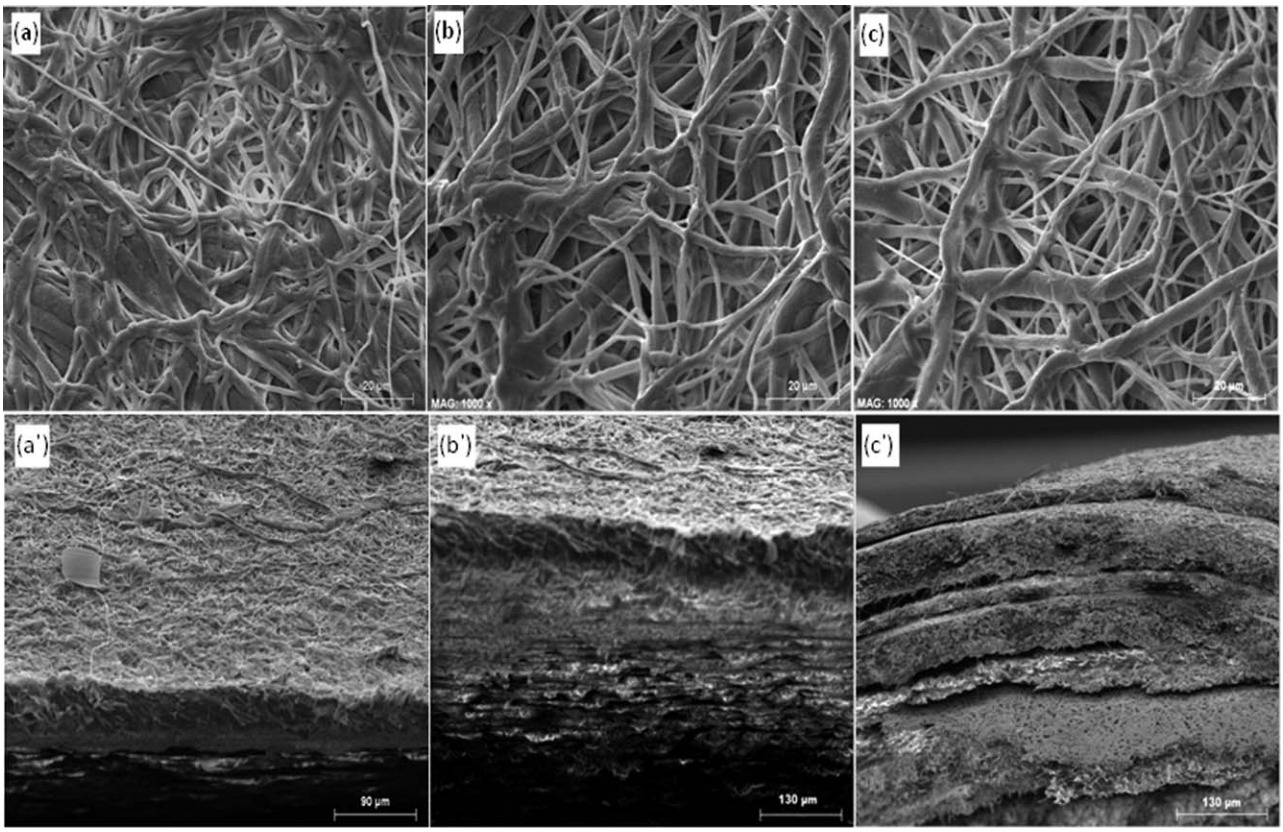

Figure 3. SEM images of surface (a–c) and cross-section (a′–c′) of electrospun PCL/PCM fibers: (a–a′) nonstored slabs, (b–b′) stored slabs for 3 months at 4°C, (c–c′) stored slabs for 3 months.

internal parts of PS/PCM slabs, the melting temperature was not significantly affected by the storage temperature and time. However, in the external parts of the paraffin-containing PS structures, the melting temperature increased during storage at 25°C. Regarding the melting and crystallization enthalpies, a slight decrease was observed with time upon storage at 25°C (in both the internal and external parts of the slabs), which again could be explained by a partial diffusion out of the PCM.

In contrast with the similarities in the melting temperature between pure RT5 and encapsulated PCM, the crystallization event was considerably different. While pure RT5 crystallizes at −5.26°C, a greater supercooling degree was observed in both internal and external zones of the PS/PCM slabs. The supercooling effect was probably due to the reduction of the PCM particle size, because the number of nuclei needed to initiate the crystallization process decreased with reducing the diameter of the RT5 drops inside the fibers. Moreover, a multiple crystallization profile was seen for the encapsulated PCM and, specifically, three crystallization temperatures were detected for the slabs. This can be mainly ascribed to the different diameter of PCM droplets.[17,18] Zhang et al.[19] assigned the multiple crystallization processes of the N-alkanes to the rotator phase transition, which is observed in these paraffins when their particle size is reduced. A rotator phase is defined as lamellar crystals, which exhibit long-range order in the molecular axis orientation and centre-of-mass position but lack rotational degrees of freedom of the molecules about their long axis. In these cases, more than one peak is observed in the DSC analysis during the crystallization process that corresponds to the different crystallization mechanisms followed. The first peak belongs to the heterogeneously nucleated liquid-rotator transition, the second one includes the rotator-crystal transition, and the last one is attributed to the homogeneously nucleated liquid-crystal transition.[18]

These multiple crystallization profile can be related with the particle size of RT5 droplets. As commented on above, the encapsulation of RT5 led to the formation of pores inside PCL or PS fibers, which were larger for PCL fibers. However, it

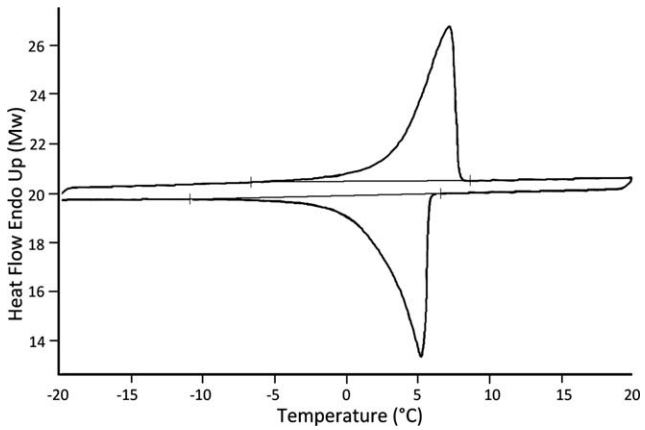

Figure 4. DSC thermograms of Rubitherm 5.

Table I. Thermal Properties of the Internal Part of PS/RT5 Slabs

Time (days)	T_{m1} (°C)		ΔH_m (J/g PCM)		T_{c1} (°C)		T_{c2} (°C)		T_{c3} (°C)		ΔH_c (J/g PCM)		Supercooling (°C)	
	4°C	25°C	4°C	25°C	4°C	25°C	4°C	25°C	4°C	25°C	4°C	25°C	4°C	25°C
0	7.3 (0.1)^{a,1}	7.4 (0.1)^{a,1}	119 (2)^{a,1}	119 (2)^{a,b,1}	9.1 (0.1)^{a,1}	9.1 (0.1)^{a,1}	5.0 (0.1)^{a,1}	5.0 (0.1)^{a,b,1}	−9.6 (0.1)^{a,1}	−9.6 (0.1)^{a,1}	117 (1)^{a,b,1}	117 (1)^{a,b,1}	2.4 (0.1)^{a,1}	2.7 (0.1)^{a,1}
7	7.1 (0.3)^{a,1}	7.5 (0.1)^{a,1}	122 (2)^{b,1}	120 (1)^{b,1}	9.0 (0.2)^{a,1}	9.3 (0.1)^{a,1}	4.5 (0.2)^{b,c,d,1}	5.2 (0.1)^{a,b,2}	−10.4 (0.2)^{b,c,1}	−10.6 (0.1)^{a,1}	121 (5)^{b,c,1}	121 (2)^{c,1}	2.6 (0.1)^{a,1}	2.4 (0.1)^{a,1}
15	6.8 (0.7)^{a,1}	7.3 (0.7)^{a,1}	128 (2)^{d,1}	121 (3)^{a,b,1}	8.9 (0.4)^{a,1}	9.2 (0.6)^{a,1}	4.5 (0.3)^{b,c,1}	5.1 (0.4)^{a,b,1}	−10.6 (0.5)^{b,1}	−10.5 (0.5)^{a,1}	129 (5)^{c,1}	119 (3)^{b,c,1}	2.4 (0.5)^{a,1}	2.3 (0.3)^{a,1}
30	6.9 (0.1)^{a,1}	7.4 (0.1)^{a,1}	125 (2)^{c,d,1}	131 (5)^{c,1}	8.7 (0.1)^{a,1}	9.2 (0.2)^{a,2}	4.3 (0.1)^{b,1}	5.0 (0.1)^{a,b,2}	−10.4 (0.1)^{b,c,1}	−10.6 (0.4)^{a,1}	125 (1)^{b,c,1}	130 (3)^{d,1}	2.6 (0.1)^{a,1}	2.4 (0.1)^{a,1}
45	7.0 (0.1)^{a,1}	7.2 (0.5)^{a,1}	115 (2)^{a,b,1}	114 (2)^{a,b,1}	8.7 (0.1)^{a,1}	9.0 (0.3)^{a,1}	4.4 (0.1)^{b,1}	4.7 (0.4)^{a,1}	−10.4 (0.6)^{b,c,1}	−10.4 (0.1)^{a,1}	117 (1)^{a,b,1}	118 (1)^{a,b,1}	2.6 (0.1)^{a,1}	2.4 (0.1)^{a,1}
60	7.2 (0.2)^{a,1}	7.3 (0.1)^{a,1}	112 (3)^{a,1}	114 (1)^{a,d,1}	8.9 (0.1)^{a,1}	9.0 (0.1)^{a,1}	4.6 (0.1)^{b,c,a,1}	4.9 (0.1)^{a,b,2}	−9.7 (0.4)^{b,c,1}	−10.1 (0.1)^{a,1}	113 (3)^{b,d,1}	116 (4)^{a,d,1}	2.7 (0.3)^{a,1}	2.4 (0.1)^{a,1}
75	7.4 (0.4)^{a,1}	7.5 (0.3)^{a,1}	113 (2)^{a,b,1}	114 (1)^{a,d,1}	9.0 (0.3)^{a,1}	9.2 (0.2)^{a,1}	4.8 (0.1)^{a,d,1}	5.1 (0.1)^{a,b,1}	−9.8 (0.4)^{a,b,1}	−9.9 (0.2)^{a,1}	118 (2)^{b,d,1}	116 (2)^{a,d,1}	2.6 (0.2)^{a,1}	2.4 (0.2)^{a,1}
90	7.2 (0.1)^{a,1}	7.4 (0.2)^{a,1}	110 (1)^{a,1}	111 (1)^{d,1}	-	-	4.7 (0.2)^{a,c,d,1}	5.2 (0.1)^{b,1}	−9.9 (0.2)^{a,b,c,1}	−9.2 (0.2)^{a,1}	112 (4)^{d,1}	111 (1)^{d,1}	2.5 (0.3)^{a,1}	2.2 (0.3)^{a,1}

a–e: Different superscripts within the same column indicate significant differences due to storage time ($P < 0.05$); 1 and 2: Different superscripts within the same line indicate significant differences due to the temperature used ($P < 0.05$).
Mean value (standard deviation).

Table II. Thermal Properties of the External Face of the PS/RT5 Slabs

Time (days)	T_{m1} (°C)		ΔH_m (J/g PCM)		T_{c1} (°C)		T_{c2} (°C)		T_{c3} (°C)		ΔH_c (J/g PCM)		Supercooling (°C)	
	4°C	25°C	4°C	25°C	4°C	25°C	4°C	25°C	4°C	25°C	4°C	25°C	4°C	25°C
0	6.9 (0.1)^{a,1}	6.8 (0.1)^{a,2}	69 (1)^{a,1}	69 (1)^{a,1}	9.1 (0.1)^{a,1}	9.6 (0.1)^{a,2}	4.1 (0.1)^{a,1}	4.1 (0.1)^{a,1}	−9.8 (0.1)^{a,b,c,1}	−9.1 (0.1)^{a,2}	71 (1)^{a,b,1}	68 (1)^{a,b,2}	2.8 (0.1)^{a,1}	2.7 (0.1)^{a,1}
7	7.0 (0.2)^{a,1}	7.5 (0.3)^{a,b,1}	70 (2)^{a,b,1}	68 (1)^{a,b,1}	9.2 (0.2)^{b,1}	9.1 (0.8)^{a,d,2}	4.3 (0.2)^{a,1}	4.6 (0.4)^{b,c,1}	−9.5 (0.4)^{b,c,1}	−9.1 (0.1)^{a,1}	70 (1)^{a,b,1}	68 (2)^{a,b,c,1}	2.7 (0.1)^{a,1}	2.9 (0.1)^{a,1}
15	7.1 (0.3)^{a,1}	7.4 (0.1)^{a,b,1}	69 (1)^{a,b,1}	62 (1)^{c,2}	9.3 (0.2)^{b,c,d,1}	9.1 (0.1)^{c,1}	4.5 (0.6)^{a,1}	4.5 (0.1)^{a,b,1}	−9.7 (0.1)^{a,b,c,1}	−9.0 (0.3)^{a,b,1}	69 (1)^{a,1}	64 (1)^{a,c,d,1}	2.5 (0.1)^{a,1}	2.9 (0.1)^{a,1}
30	7.4 (0.1)^{b,c,1}	7.7 (0.6)^{b,1}	73 (3)^{b,1}	70 (4)^{a,1}	9.6 (0.2)^{c,d,1}	9.5 (0.3)^{a,d,1}	4.8 (0.5)^{a,1}	4.7 (0.2)^{b,c,d,1}	−9.5 (0.2)^{a,b,c,1}	−9.0 (0.4)^{a,b,1}	76 (1)^{b,1}	71 (1)^{b,1}	2.7 (0.5)^{a,1}	3.0 (0.4)^{a,1}
45	7.2 (0.1)^{a,b,c,1}	7.5 (0.1)^{a,b,1}	74 (2)^{b,1}	64 (2)^{b,c,2}	9.2 (0.1)^{b,c,1}	9.3 (0.1)^{c,d,1}	4.5 (0.3)^{a,1}	4.6 (0.1)^{a,b,1}	−9.9 (0.1)^{a,b,1}	−9.6 (0.1)^{a,b,c,2}	76 (1)^{b,1}	62 (1)^{c,d,1}	2.7 (0.3)^{a,1}	2.9 (0.1)^{a,1}
60	7.6 (0.2)^{c,1}	7.6 (0.2)^{a,b,1}	71 (2)^{a,b,1}	63 (1)^{c,2}	9.6 (0.1)^{d,1}	9.4 (0.1)^{a,d,1}	4.8 (0.1)^{a,1}	5.0 (0.1)^{c,d,1}	−9.3 (0.1)^{c,1}	−8.5 (0.5)^{a,b,c,1}	72 (5)^{b,1}	59 (4)^{a,c,d,1}	2.7 (0.1)^{a,1}	2.6 (0.1)^{a,1}
75	7.2 (0.2)^{a,b,1}	7.7 (0.6)^{b,1}	72 (4)^{a,b,1}	59 (2)^{c,1}	8.9 (0.1)^{b,1}	9.9 (0.1)^{b,2}	4.4 (0.5)^{a,1}	5.0 (0.1)^{c,d,1}	−9.6 (0.2)^{a,b,c,1}	−8.4 (0.1)^{b,c,1}	69 (5)^{a,b,1}	62 (1)^{a,c,d,1}	2.7 (0.6)^{a,1}	2.6 (0.6)^{a,1}
90	7.0 (0.1)^{a,1}	7.9 (0.2)^{b,2}	69 (1)^{a,b,1}	59 (4)^{c,1}	9.0 (0.2)^{a,1}	9.8 (0.2)^{a,1}	4.4 (0.7)^{a,1}	5.1 (0.2)^{d,1}	−9.9 (0.1)^{a,1}	−8.3 (0.6)^{c,1}	69 (1)^{a,1}	60 (3)^{d,2}	2.6 (0.6)^{a,1}	2.8 (0.1)^{a,1}

a–d: Different superscripts within the same column indicate significant differences due to storage time ($P < 0.05$); 1 and 2: Different superscripts within the same line indicate significant differences due to the temperature used ($P < 0.05$).
Mean value (standard deviation).

Table III. Thermal Properties of the Internal Part of PCL/RT5 Slabs

Time (days)	T_{m1} (°C)		ΔH_m (J/g PCM)		T_{c1} (°C)		T_{c2} (°C)		ΔH_c (J/g PCM)		Supercooling (°C)	
	4°C	25°C	4°C	25°C	4°C	25°C	4°C	25°C	4°C	25°C	4°C	25°C
0	7.7 (0.1)^{a,1}	7.3 (0.5)^{a,b,1}	131 (1)^{a,1}	131 (1)^{a,1}	5.4 (0.1)^{a,1}	5.3 (0.2)^{a,1}	1.8 (0.1)^{a,1}	1.8 (0.1)^{a,1}	130 (1)^{a,1}	130 (1)^{a,1}	2.3 (0.1)^{a,1}	2.0 (0.3)^{a,1}
7	7.6 (0.1)^{a,1}	7.6 (0.5)^{a,b,1}	132 (1)^{a,1}	126 (1)^{a,b,2}	5.4 (0.1)^{a,1}	5.4 (0.3)^{a,b,1}	1.9 (0.1)^{a,b,1}	2.0 (0.1)^{b,1}	131 (1)^{a,b,1}	127 (2)^{b,2}	2.2 (0.1)^{b,c,1}	2.2 (0.5)^{a,1}
15	7.6 (0.3)^{a,1}	7.8 (0.1)^{a,b,1}	135 (4)^{a,1}	126 (1)^{a,b,2}	5.3 (0.4)^{a,1}	5.7 (0.1)^{b,1}	2.0 (0.2)^{b,c,1}	2.6 (0.1)^{c,2}	137 (4)^{d,e,1}	125 (1)^{b,2}	2.3 (0.1)^{a,b,1}	2.1 (0.1)^{a,b,1}
30	7.6 (0.3)^{a,1}	8.1 (0.3)^{b,1}	138 (3)^{a,b,1}	121 (1)^{b,2}	5.5 (0.3)^{a,b,1}	6.1 (0.1)^{c,2}	2.1 (0.2)^{b,c,d,1}	3.9 (0.2)^{d,2}	136 (1)^{c,d,1}	120 (1)^{c,2}	2.1 (0.1)^{a,b,1}	2.0 (0.3)^{a,b,1}
45	7.6 (0.1)^{a,1}	8.1 (0.1)^{b,1}	135 (3)^{b,c,1}	121 (1)^{b,2}	5.5 (0.1)^{a,b,1}	6.3 (0.2)^{d,2}	2.2 (0.1)^{c,d,e,1}	4.1 (0.1)^{d,e,2}	135 (1)^{b,c,d,1}	116 (3)^{d,2}	2.1 (0.1)^{b,c,1}	1.8 (0.1)^{a,b,2}
60	7.5 (0.1)^{a,1}	8.1 (0.2)^{b,1}	140 (1)^{c,1}	120 (3)^{b,2}	5.5 (0.1)^{a,b,1}	6.5 (0.2)^{d,2}	2.3 (0.1)^{d,e,1}	4.2 (0.1)^{e,2}	141 (2)^{e,1}	118 (2)^{c,d,2}	2.1 (0.1)^{b,1}	1.7 (0.1)^{a,b,2}
75	7.3 (0.1)^{a,1}	8.1 (0.1)^{a,1}	137 (1)^{d,1}	107 (1)^{c,2}	5.5 (0.1)^{a,b,1}	6.5 (0.1)^{d,2}	2.2 (0.1)^{c,d,e,1}	4.2 (0.2)^{e,2}	138 (1)^{d,e,1}	108 (1)^{e,2}	1.8 (0.1)^{c,1}	1.6 (0.2)^{a,b,1}
90	7.6 (0.1)^{a,1}	8.3 (0.6)^{a,b,1}	133 (1)^{d,1}	106 (4)^{c,2}	5.6 (0.1)^{b,1}	6.5 (0.1)^{d,2}	2.4 (0.1)^{e,1}	4.2 (0.1)^{e,2}	133 (1)^{a,b,c,1}	106 (3)^{e,2}	1.7 (0.1)^{c,1}	1.6 (0.3)^{b,1}

a–e: Different superscripts within the same column indicate significant differences due to storage time ($P < 0.05$); 1 and 2: Different superscripts within the same line indicate significant differences due to the temperature used ($P < 0.05$).
Mean value (standard deviation).

Table IV. Thermal Properties of the External Face of the PCL/RT5 Slabs

Time (days)	T_{m1} (°C)		ΔH_m (J/g PCM)		T_{c1} (°C)		T_{c2} (°C)		ΔH_c (J/g PCM)		Supercooling (°C)	
	4°C	25°C	4°C	25°C	4°C	25°C	4°C	25°C	4°C	25°C	4°C	25°C
0	7.5 (0.1)^{a,1}	7.5 (0.1)^{a,1}	110 (1)^{a,b,1}	110 (1)^{a,b,1}	5.5 (0.1)^{a,1}	5.5 (0.1)^{a,1}	2.0 (0.1)^{a,1}	2.0 (0.1)^{a,1}	109 (1)^{a,1}	109 (1)^{a,b,1}	2.0 (0.1)^{a,1}	2.1 (0.1)^{a,1}
7	7.2 (0.1)^{a,1}	7.6 (0.1)^{a,2}	107 (1)^{a,1}	107 (1)^{a,b,c,1}	5.0 (0.1)^{a,1}	5.5 (0.1)^{a,2}	1.9 (0.1)^{a,1}	2.3 (0.1)^{a,b,2}	111 (1)^{a,b,1}	106 (1)^{b,1}	2.2 (0.1)^{a,1}	2.1 (0.1)^{a,2}
15	7.4 (0.1)^{a,1}	7.8 (0.1)^{b,2}	114 (3)^{b,c,1}	103 (1)^{a,c,2}	5.3 (0.1)^{a,1}	5.7 (0.1)^{b,2}	1.9 (0.6)^{a,1}	2.9 (0.1)^{b,2}	115 (4)^{b,c,1}	105 (1)^{a,1}	2.1 (0.1)^{a,1}	2.1 (0.1)^{a,1}
30	7.5 (0.2)^{a,1}	8.0 (0.1)^{b,1}	124 (5)^{d,1}	106 (2)^{a,c,2}	5.5 (0.1)^{a,1}	6.1 (0.1)^{c,1}	2.5 (0.7)^{a,1}	4.1 (0.5)^{c,2}	123 (4)^{d,e,1}	108 (1)^{a,b,2}	2.1 (0.1)^{a1}	1.9 (0.2)^{a,b,1}
45	7.5 (0.2)^{a,1}	8.0 (0.2)^{b,c,1}	114 (1)^{b,c,1}	111 (4)^{b,1}	5.3 (0.4)^{a,1}	6.3 (0.2)^{d,2}	3.6 (0.1)^{b,1}	4.5 (0.2)^{c,d,2}	115 (2)^{b,c,1}	112 (4)^{b,1}	2.2 (0.1)^{a,1}	1.7 (0.4)^{b,c,2}
60	7.6 (0.1)^{a,1}	8.1 (0.2)^{b,c,1}	118 (3)^{c,1}	101 (1)^{d,2}	5.4 (0.1)^{a,1}	6.5 (0.1)^{d,e,2}	4.6 (0.1)^{c,1}	4.7 (0.1)^{c,d,2}	118 (2)^{c,d,1}	99 (3)^{c,2}	2.2 (0.2)^{a,1}	1.7 (0.2)^{b,c,2}
75	7.5 (0.3)^{a,1}	8.0 (0.2)^{b,c,1}	124 (1)^{d,1}	99 (3)^{d,2}	5.3 (0.3)^{a,1}	6.5 (0.7)^{e,2}	4.3 (0.2)^{b,c,1}	4.7 (0.6)^{c,d,2}	127 (2)^{e,1}	96 (3)^{c,2}	2.2 (0.1)^{a,1}	1.5 (0.9)^{c,2}
90	7.7 (0.4)^{a,1}	8.3 (0.1)^{c,1}	115 (2)^{b,c,1}	100 (2)^{d,2}	5.4 (0.3)^{a,1}	6.7 (0.1)^{f,2}	4.7 (0.8)^{d,1}	4.7 (0.1)^{d,2}	114 (2)^{a,b,c,1}	97 (3)^{c,2}	2.2 (0.1)^{a,1}	1.5 (0.1)^{c,2}

a–e: Different superscripts within the same column indicate significant differences due to storage time ($P < 0.05$); 1 and 2: Different superscripts within the same line indicate significant differences due to the temperature used ($P < 0.05$).
Mean value (standard deviation).

J. APPL. POLYM. SCI. 2014, DOI: 10.1002/APP.40661

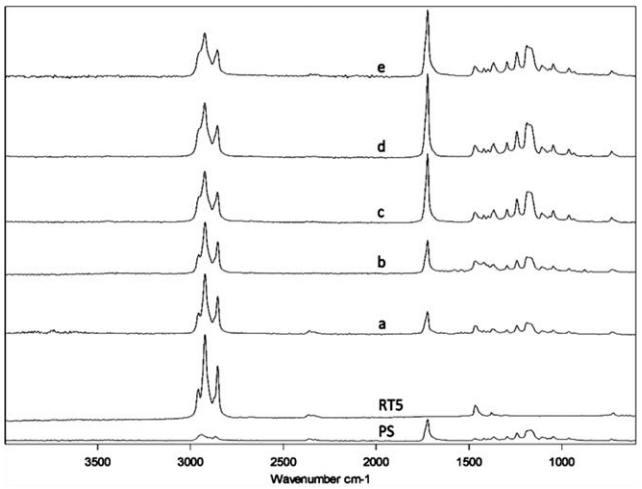

Figure 5. ATR-FTIR spectra of the pure PS polymer, pure RT5, and non-stored and stored PS/PCM hybrid electrospun materials measured at 4°C and 25°C, at the internal and external part of the slabs. (a) PS/RT5 non-stored slabs, (b) and (c) internal PS/RT5 slabs stored for 3 months at 4°C and 25°C, respectively, as well as (d) and (e) external PS/RT5 slabs stored for 3 months at 4°C and 25°C, respectively.

appears that microemulsions were formed during the preparation of PS-based solutions, leading to the formation of smaller pores within the electrospun fibers, which resulted in the heterogeneous crystallization phenomena observed. Similar to that observed for PS/PCM slabs, there were not significant changes between the melting temperatures of pure RT5 and PCL/RT5 slabs. It is important to note that the melting enthalpy of PCL/RT5 slabs was significantly higher than that of PS/RT5 slabs, fact which could also be attributed to a greater encapsulation efficiency probably related with the larger size of PCL/RT5 fibers. Once again and probably as a result of the heat-treatment used for the formation of slabs, melting and crystallization enthalpies were lower at the external parts of the PCL/PCM slabs. The melting temperature as well as melting and crystallization enthalpies did not vary significantly in PCL/PCM slabs stored at 4°C. However, a significant increase in the melting temperature together with a decrease in the melting and crystallization enthalpies were observed in PCL/RT5 slabs stored at 25°C. This could be ascribed to the PCM diffusion throughout the PCL matrix along storage.

Two crystallization temperatures were detected for the PCL/PCM slabs which can be assigned to the crystallization behavior of lamellar crystals described above, with the second and third transitions appearing as a single peak.[19] These differences between PCL and PS crystallization behavior could be also explained by the different particle size of the PCM droplets, which was greater in PCL fibers. Similar behavior was observed in PCL/dodecane hybrid structures.[9]

The presence of PCM in the slabs was also qualitatively evaluated by ATR-FTIR spectroscopy. Figure 5 shows the ATR-FTIR spectra of the pure PS fibers, the pure RT5, and the PS/RT5 slabs analyzed at 20°C. At this temperature, the pure RT5 is characterized by the $-CH_2$ and $-CH_3$ stretching vibration bands at 2956, 2922, and 2854 cm^{-1}. These bands were also observed in the PS/RT5 slabs even though they were overlapped with the spectral bands from the PS, thus confirming the PCM encapsulation in the PS matrix. It is worth noting that the intensity of the characteristic bands from the paraffin was greater at the internal part of the slabs and decreased in those stored at 25°C (Table V). This is directly related with the enthalpy values commented on above because higher intensity of the characteristic bands from the PCM means higher encapsulation efficiency which were closely related with higher melting enthalpy values. Thus, the crystallization and melting enthalpy of slabs were significantly higher at the internal part of the slabs, probably due to the slight heat-treatment suffered from the outer zones during the slab-formation. Moreover, the decrease in the intensity of the characteristic bands from the

Table V. Ratio of RT5 and PS or PCL

	Bands intensity			
Material	2921,87 cm^{-1}	698,16 cm^{-1}	1724,19 cm^{-1}	Ratio (RT5/PS or PCL)
Rubitherm 5 (RT5)	1.0354	-		-
Polystyrene (PS)	0.0519	0.0898		0.5778
PS/RT5 nonstored slabs	0.1369	0.0773		1.7711
Internal PS/RT5 slabs stored for 3 months at 4°C	0.0998	0.1029		0.9696
Internal PS/RT5 slabs stored for 3 months at 25°C	0.0766	0.0824		0.9289
External PS/RT5 slabs stored for 3 months at 4°C	0.0576	0.0761		0.7573
External PS/RT5 slabs stored for 3 months at 25°C	0.0364	0.0613		0.5939
Polycaprolactone (PCL)	0.0604		0.2551	0.2368
PCL/RT5 nonstored slabs	0.7090		0.2770	2.5594
Internal PCL/RT5 slabs stored for 3 months at 4°C	0.6613		0.4499	1.4699
Internal PCL/RT5 slabs stored for 3 months at 25°C	0.5996		0.7988	0.7505
External PCL/RT5 slabs stored for 3 months at 4°C	0.6227		0.9574	0.6504
External PCL/RT5 slabs stored for 3 months at 25°C	0.5521		0.8312	0.6642

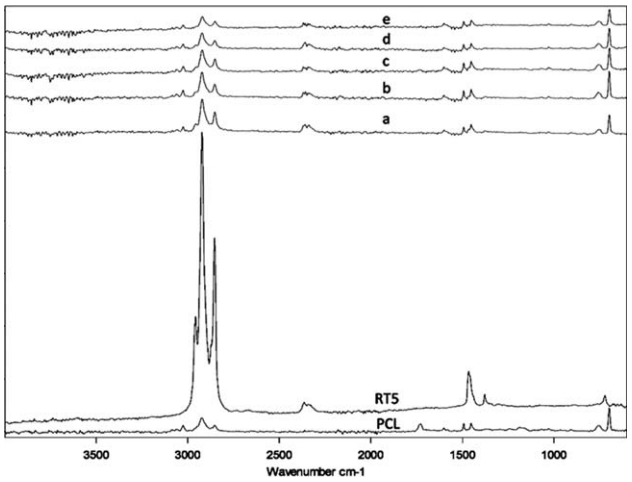

Figure 6. ATR-FTIR spectra of the pure PCL polymer, pure RT5, and nonstored and stored PCL/PCM hybrid electrospun materials measured at 4°C and 25°C, at the internal and external part of the slabs. (a) PCL/RT5 nonstored slabs, (b) and (c) internal PCL/RT5 slabs stored for 3 months at 4°C and 25°C, respectively, as well as (d) and (e) external PCL/RT5 slabs stored for 3 months at 4°C and 25°C, respectively.

PCM in the slabs stored at 25°C were closely related with the partial diffusion out of the paraffin and thus, with the lower melting enthalpy values found in the stored slabs.

Figure 6 compares the ATR-FTIR spectra of the pure PCL fibers, the pure PCM, and the internal and external parts of the nonstored and stored PCL/RT5 slabs analyzed at 20°C. Once again, the —CH_2 and —CH_3 stretching vibration bands at 2956, 2922, and 2854 cm^{-1} appeared in all PCL/RT5 slabs even though they were also overlapped with the spectral bands of PCL. Similarly to that observed for the PS-based slabs, the relative intensity of the PCM bands with respect to the polymer ones was greater both in the internal parts of the slab and upon storage at 4°C (Table V). Again, these results are in agreement with enthalpy values.

Evaluation of the PCM Encapsulation Efficiency and Loading

The PCM encapsulation efficiency and loading capacity of the hybrid structures were evaluated from the enthalpy results obtained through DSC. The encapsulation yield was calculated by dividing the experimental by the expected theoretical melting enthalpies obtained for PS or PCL materials. The theoretical melting enthalpy was obtained considering the quantity of RT5 added to the electrospinning solution (45 wt %) and multiplying this by the experimental enthalpy of the pure RT5. Figures 7 and 8 show the encapsulation efficiency and the calculated total amount of the PCM encapsulated in the PS and PCL slabs, respectively. Both (internal and external) parts of slabs stored at 4 and 25°C were analyzed.

PCL structures presented greater encapsulation efficiency than PS and the encapsulation yield was always higher at the internal part of the slabs, as previously anticipated by the thermal and morphological characterization. The greater encapsulation efficiency of PCL structures could be related with the greater diameter and internal structure observed in these fibers which could retain a higher amount of the PCM. A similar behavior was also observed by Pérez-Masiá et al.[9] working with PCL/

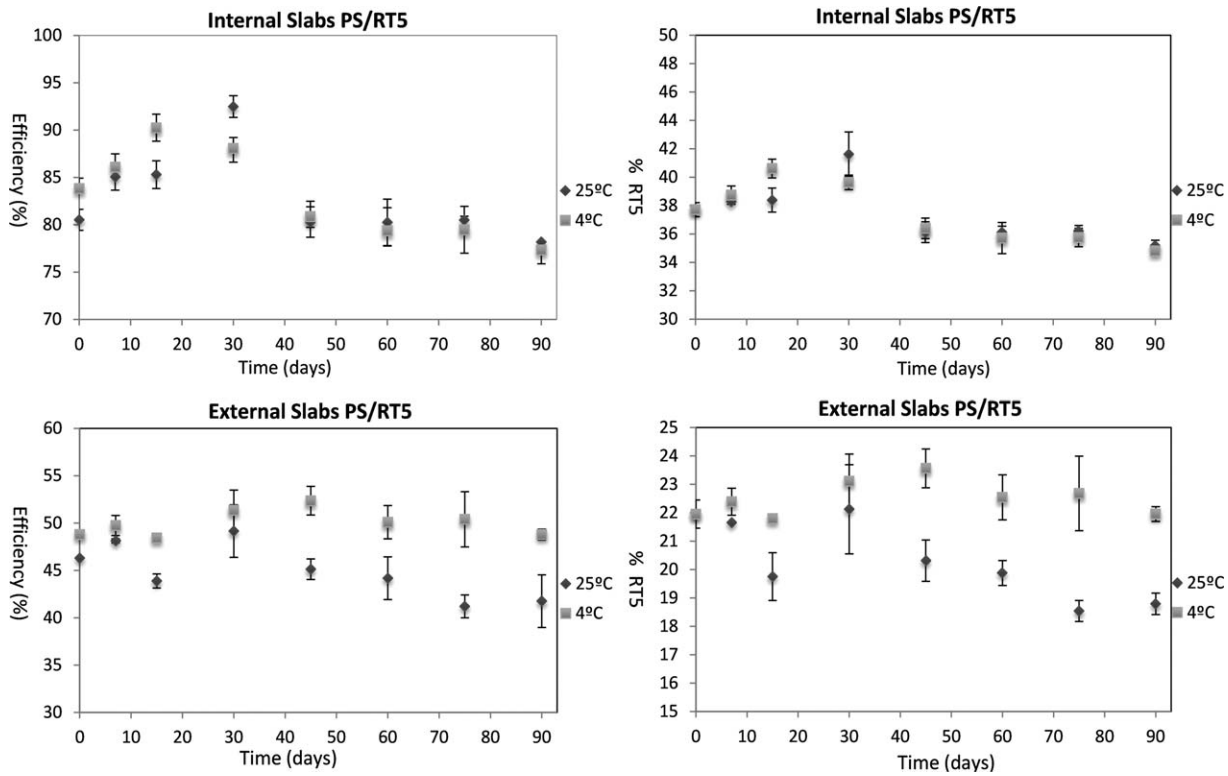

Figure 7. Encapsulation efficiency and the calculated amount of the RT5 (%) encapsulated in the PS fibers during ageing at 4°C and 25°C.

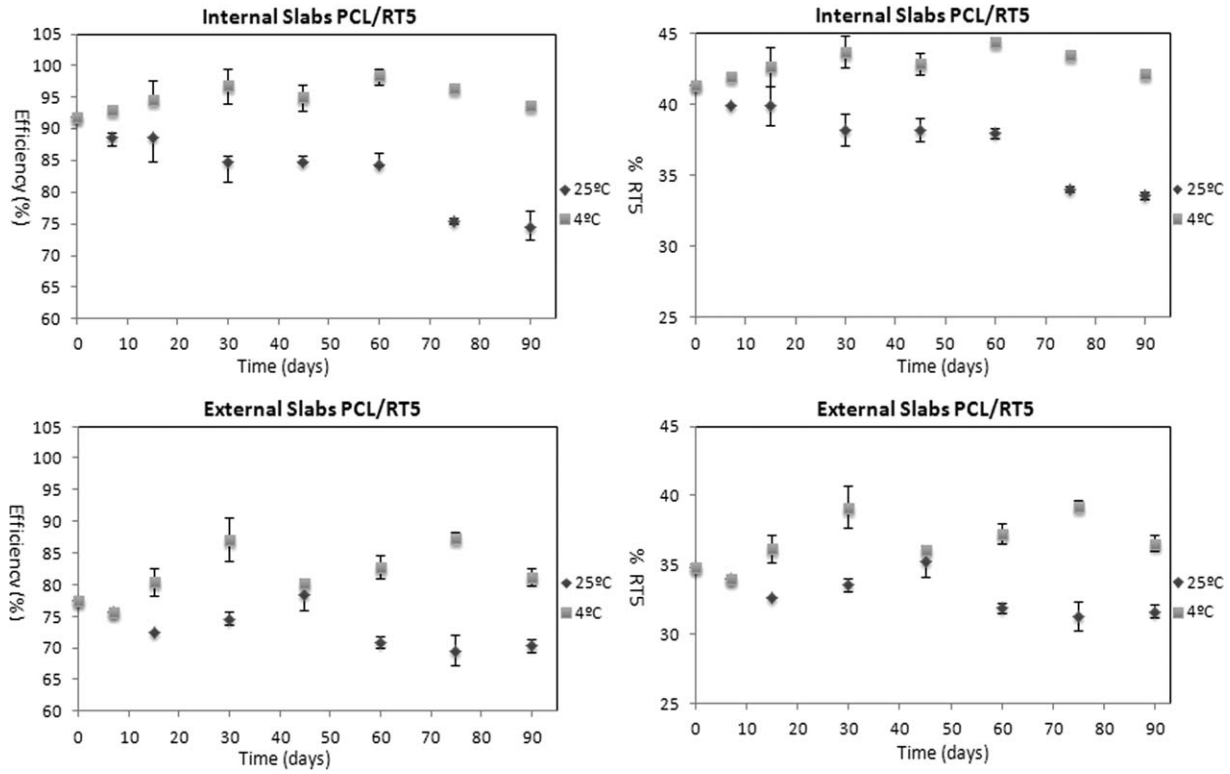

Figure 8. Encapsulation efficiency and the calculated amount of the RT5 (%) encapsulated in the PCL fibers at 4°C and 25°C.

dodecane (porous fibers) and PLA/dodecane hybrid structures (thinner and nonporous fibers).

On the other hand, the lower encapsulation efficiency observed in the outer layers was probably related with the slight heat-treatment used for the formation of the PCL/PCM and PS/PCM slabs. It may be noted that the encapsulation yield at the external part of the slabs significantly decreased with the storage time at 25°C probably due to the partial diffusion out of the paraffin during ageing (which was in liquid state at this temperature). However, the internal part of the hybrid structures behaved differently depending on the matrix and temperature used. For instance, the encapsulation efficiency in the PS/RT5 hybrid structures decreased by up to 14.90% for the internal part of slabs stored at 90 days, having not significantly differences between those stored at 4°C or 25°C. This was more noticeable in the case of the internal part of the PCL/PCM structures stored at 25°C, where the encapsulation efficiency decreased by up to 18.86% for slabs stored 90 days. However, no significant variations were observed in the PCL/PCM structures stored at 4°C. As commented on above, this could be attributed to the

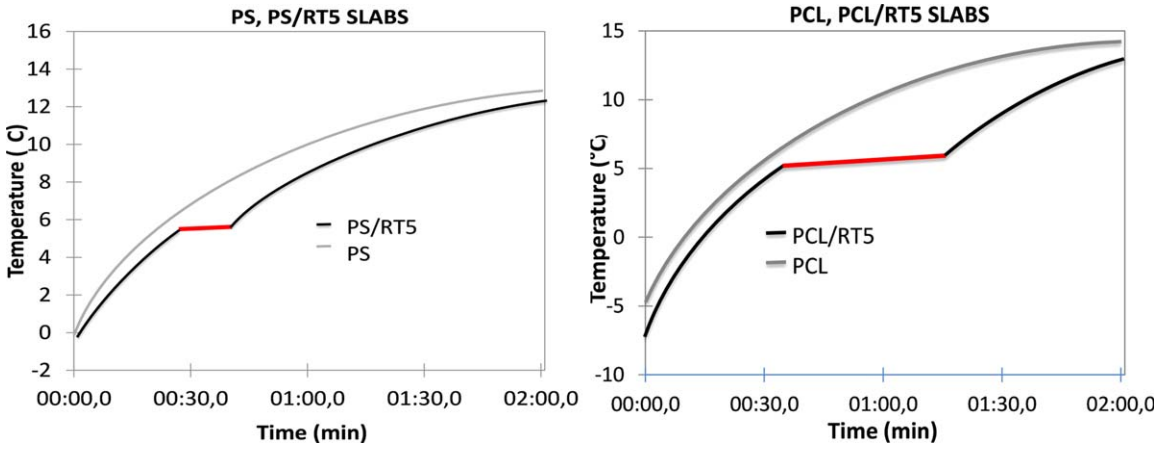

Figure 9. Surface temperature as a function of time for PS/PCM (a) and PCL/PCM (b) slabs. [Color figure can be viewed in the online issue, which is available at wileyonlinelibrary.com.]

different physical state of the PCM at 4°C and 25°C together with the porous structures of PCL fibers.

From the results, it can be concluded that the greatest encapsulation efficiency (98.56%) was achieved for PCL/PCM slabs stored at 4°C, which retained the encapsulated PCM during storage and were thus composed of 44.35 wt % of PCM (the core material) and 55.65 wt % of the PCL shell material.

Temperature Profile of PS/PCM and PCL/PCM Slabs

The thermal behavior of the PCM was also evaluated by recording the temperature profiles of PCL and PS slabs stored at −18°C and analyzed at room temperature (20°C). Figure 9 compares the temperature profiles of the PS/PCM (a) and PCL/PCM (b) slabs with their counterparts without PCM, as they pass through the melting range of RT5. The IR probe is expected to provide thermal information mostly coming from the surface of the material where lower encapsulation efficiency values were observed.

As expected, the increased effective specific heat over the melting region has the effect of slowing down the rate of temperature rise locally. In both cases, the slope of the time-temperature curve of the PCL/PCM and PS/PCM slabs decreased and even plateau for some time in the melting range of the PCM for both encapsulation structures, but it was more pronounced in the PCL hybrid structures, which could thus be more effective at temperature buffering.

CONCLUSIONS

In this work, heat management materials based on the encapsulation of a PCM (RT5) inside PS or PCL were successfully developed. Melting behavior of the encapsulated RT5 was similar to that of pure RT5. However, a multiple crystallization profile was observed for the encapsulated PCM. While pure RT5 crystallizes at −5.26°C, a greater supercooling degree was observed in both internal and external zones of the PS/PCM and PCL/PCM slabs, probably due to the reduction of the PCM particle size.

Results showed that PCL/PCM slabs were able to encapsulate a greater amount of the RT5 than those obtained with PS. The encapsulation efficiency decreased in the PS/PCM and PCL/PCM slabs stored at 25°C which was attributed to the progressive diffusion out of the PCM from the capsules during aging (which was in liquid state at this temperature). However, no significant changes during aging were observed in those stored at 4°C, showing that PCL/PCM slabs stored at 4°C had the greatest encapsulation efficiency (98.56%). Therefore, the developed PCL/PCM hybrid structures would be able to encapsulate a heat storage capacity equivalent to ~44 wt % of PCM, at 4°C for at least 3 months.

ACKNOWLEDGMENTS

The authors acknowledge financial support from EU project of the FP7 FRISBEE for financial support. W. Chalco-Sandoval thanks to SENESCYT for the pre-doctoral grant. A. Lopez-Rubio and M. J. Fabra are recipients of a Ramon y Cajal contract and a Juan de la Cierva contract from the Spanish Ministry of Economy and Competitivity, respectively.

REFERENCES

1. Jin, Y.; Lee, W.; Musina, Z.; Ding, Y. *Particuology* **2010**, *8*, 588.
2. Oró, E.; de Gracia, A.; Castell, A.; Farid, M. M.; Cabeza, L. F. *Appl. Energy* **2012**, *99*, 513.
3. Farid, M. M.; Khudhair, A.; Razack, S. A. K.; Al-Hallaj, S. A. *Energy Convers. Manage.* **2004**, *45*, 1597.
4. Sharma, A.; Tyagi, V. V.; Chen, C. R.; Buddhi, D. *Renew. Sust. Energy Rev.* **2009**, *13*, 318.
5. Alkan, C.; Sarı, A.; Karaipekli, A. *Energy Convers. Manage.* **2011**, *52*, 687.
6. Fang, G.; Li, H.; Yang, F.; Liu, X.; Wu, S. *Chem. Eng. J.* **2009**, *153*, 217.
7. Goldberg, M.; Langer, R.; Jia, X. *J. Biomater. Sci. Polym. Ed.* **2007**, *18*, 241.
8. Pérez-Masiá, R.; López-Rubio, A.; Lagarón, J. M. *Food Hydrocolloids* **2013**, *30*, 182.
9. Pérez-Masiá, R.; López-Rubio, A.; Fabra, M. J.; Lagaron, J. M. *J. Appl. Polym.* **2013**, *30*, 3251.
10. Teo, W. E.; Ramakrishna, S. *Nanotechnology* **2006**, *17*, R89.
11. Arecchi, A.; Mannino, S.; Weiss, J. *J. Food Sci.* **2010**, *75*, N80.
12. Huang, L.; Bui, N.; Manickam, S.; McCutcheon, J. *J. Polym. Sci. Part B: Polym. Phys.* **2011**, *49*, 1734.
13. Casper, C.; Stephens, J.; Tassi, N.; Chase, D.; Rabolt, J. *Macromolecules* **2004**, *37*, 573.
14. Medeiros, E.; Mattoso, H. C.; Offeman, D.; Wood, F.; Orts, W.; Can, J. *Can. J. Chem.* **2008**, *86*, 590.
15. Megelski, S.; Stephens, J. S.; Chase, D. B.; Rabolt, J. F. *Macromolecules* **2002**, *35*, 8456.
16. Van de Witte, P.; Dijkstra, P. J.; van den Berg, J. W.; Feijen, J. *J. Membr. Sci.* **1996**, *117*, 1.
17. Zhang, S.; Wu, J. Y.; Tse, C. T.; Niu, J. *Sol. Energy Mater. Sol. Cells* **2012**, *96*, 124.
18. Delgado, M.; Lázaro, A.; Mazo, J.; Zalba, B. *Renew. Sust. Energy Rev.* **2012**, *16*, 253.
19. Zhang, X. X.; Tao, X. M.; Yick, K. L.; Wang, X. C. *Colloid Polym. Sci.* **2004**, *282*, 330.